2016

Are Long Tide Gauge Records in the Wrong Place to Measure Global Mean Sea Level Rise?

P. R. Thompson

B. D. Hamlington
Old Dominion University, bhamling@odu.edu

F. W. Landerer

S. Adhikari

Original Publication Citation

Thompson, P. R., Hamlington, B. D., Landerer, F. W., & Adhikari, S. (2016). Are long tide gauge records in the wrong place to measure global mean sea level rise? *Geophysical Research Letters, 43*(19), 10,403-410,411. doi:10.1002/2016GL070552

AGU PUBLICATIONS

Geophysical Research Letters

RESEARCH LETTER
10.1002/2016GL070552

Key Points:
- Averaging trends from a few high-quality tide gauge records can lead to systematic underestimate or overestimate of global mean sea level rise
- The best tide gauge records tend to sample the ocean where twentieth century sea level rise was most likely less than the global mean rate
- Global mean rates less than 1.4 mm/yr are difficult to reconcile with observed trends in the longest and highest-quality tide gauge records

Supporting Information:
- Supporting Information S1
- Supporting Information S2
- Figure S1

Correspondence to:
P. R. Thompson,
philiprt@hawaii.edu

Citation:
Thompson, P. R., B. D. Hamlington, F. W. Landerer, and S. Adhikari (2016), Are long tide gauge records in the wrong place to measure global mean sea level rise?, *Geophys. Res. Lett.*, *43*, 10,403–10,411, doi:10.1002/2016GL070552.

Received 22 JUL 2016
Accepted 15 SEP 2016
Accepted article online 19 SEP 2016
Published online 9 OCT 2016

Are long tide gauge records in the wrong place to measure global mean sea level rise?

P. R. Thompson[1], B. D. Hamlington[2], F. W. Landerer[3], and S. Adhikari[3]

[1]Department of Oceanography, University of Hawai'i at Mānoa, Honolulu, Hawaii, USA, [2]Center for Coastal Physical Oceanography, Old Dominion University, Norfolk, Virginia, USA, [3]Jet Propulsion Laboratory, California Institute of Technology, Pasadena, California, USA

Abstract Ocean dynamics, land motion, and changes in Earth's gravitational and rotational fields cause local sea level change to deviate from the rate of global mean sea level rise. Here we use observations and simulations of spatial structure in sea level change to estimate the likelihood that these processes cause sea level trends in the longest and highest-quality tide gauge records to be systematically biased relative to the true global mean rate. The analyzed records have an average twentieth century rate of approximately 1.6 mm/yr, but based on the locations of these gauges, we show that the simple average underestimates the twentieth century global mean rate by 0.1 ± 0.2 mm/yr. Given the distribution of potential sampling biases, we find that <1% probability that observed trends from the longest and highest-quality tide gauge records are consistent with global mean rates less than 1.4 mm/yr.

1. Introduction

Tide gauge (TG) sea level records provide the basis for estimates of twentieth century global mean sea level (GMSL) rise. It is not straightforward, however, to infer the rate of global ocean volume change from these data, because a variety of processes cause local sea level trends to deviate from the global mean rate of change [e.g., *Douglas*, 1991]. Examples include ocean dynamics, vertical land motion, and changes in Earth's gravitational and rotational fields. In addition, the vast majority of TG records contain less than 50 years of twentieth century data, which often makes it difficult to distinguish secular sea level rise from decadal and multidecadal climate variability.

The simplest approach to address these challenges is to estimate twentieth century GMSL rise by averaging trends from only the longest and highest-quality TG records [e.g., *Douglas*, 1997; *Holgate*, 2007; *Spada and Galassi*, 2012]. In this context, "high quality" means mostly complete records that are minimally affected by (1) tectonic activity, (2) subsidence/uplift unrelated to glacial isostatic adjustment (GIA), and (3) discontinuities due to relocation or destruction/reestablishment of gauge sites. After correcting for GIA, a simple average of trends from long, high-quality records typically produces "global" rates of 1.5–1.8 mm/yr [*Douglas*, 1997; *Holgate*, 2007; *Spada and Galassi*, 2012]. Such analyses tend to treat scatter in TG trends as random error due to local and regional processes, but they generally ignore the potential for nonrandom bias error. This is an important omission, because a small number of records can systematically underestimate or overestimate the global trend due to sparse, suboptimal spatial sampling of processes that produce large-scale spatial structure in the long-term rate of sea level change [*Mitrovica et al.*, 2001].

Another approach is to combine a wider selection of TG records with information about the spatial structure of sea level change, which minimizes the potential for sampling bias [*Chambers*, 2002; *Church and White*, 2011; *Ray and Douglas*, 2011]. Most recently, a probabilistic estimate of twentieth century GMSL variability combined TG records of various lengths with information about the spatial structure and time history of dynamic and geodetic sea level change [*Hay et al.*, 2015]. This method resulted in a twentieth century global mean rate of 1.2 ± 0.2 mm/yr, which is less than the GIA-corrected observed sea level trend at most of the long, high-quality TG records.

Taken together, the above findings suggest that the best TG records are poorly located for capturing the global mean rate of change and tend to sample the ocean at locations where sea level rose faster than average during the twentieth century. In the following analysis, we use observations and simulations of spatial structure in sea level change to estimate the likelihood that ocean dynamics and/or geodetic processes result in historical

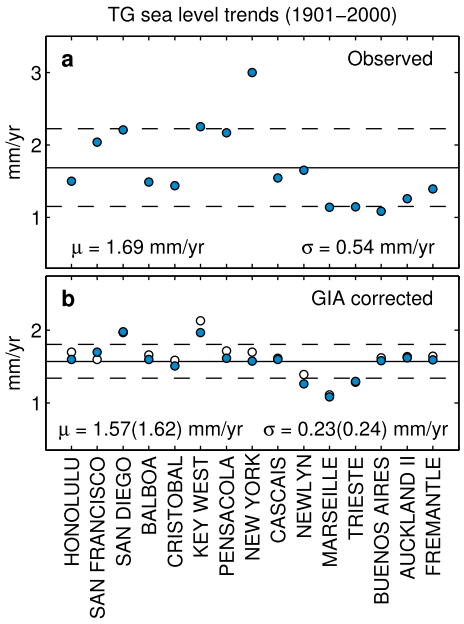

Figure 1. Least squares linear sea level trends during 1901–2000. (a) Observed. (b) Corrected for glacial isostatic adjustment (GIA) using the ICE-6G VM5a (blue) and ICE-5G VM2 (white). Solid and dashed lines in both panels represent the mean and 1σ range, respectively. In Figure 1b, the lines correspond to the ICE-6G VM5a correction; values for the mean and standard deviation using the ICE-5G VM2 correction are given in parentheses.

sea level trends in the longest and highest-quality TG records that systematically differ from the true rate of GMSL rise. We also assess how these gauges sample patterns of sea level change in order to identify which processes might reconcile observed TG trends with reconstructed global mean rates.

2. Tide Gauge Data

Studies of twentieth century sea level rise based on a small number of TGs [e.g., *Douglas*, 1997; *Holgate*, 2007; *Spada and Galassi*, 2012] employ different criteria for selecting high-quality records, which results in different (but overlapping) sets of gauges. A primary objective of this work is to understand why estimates of this type, as a whole, tend to produce estimates of GMSL rise greater than the probabilistic estimate of *Hay et al.* [2015]. Here we identify 15 of the longest, highest-quality TG records that make up the core group of TGs utilized in these types of analyses (see below).

We use annual mean TG data from the Permanent Service for Mean Sea Level (PSMSL) Revised Local Reference database [*Holgate et al.*, 2013]. PSMSL flags suspect data, and each of the 15 records chosen here contain at least 70 unflagged twentieth century annual mean values. The supporting information includes a complete description of the gauge selection process and relevant metadata for each record (Texts S1 and S2 and Table S1 in the supporting information). Figures 1 and 2 show the names and locations of the 15 records. The set of records used by *Douglas* [1997] and *Mitrovica et al.* [2001] contains 15 records with at least 70 valid annual means during 1901–2000; 13 of them are included here. The set used by *Holgate* [2007] contains 9 records; all 9 of them are included here. The set used by *Spada and Galassi* [2012] contains 11 non-Baltic/Black Sea records with at least 70 valid annual means during 1901–2000; 9 of them are included here. We exclude Baltic and Black Sea gauges, because these

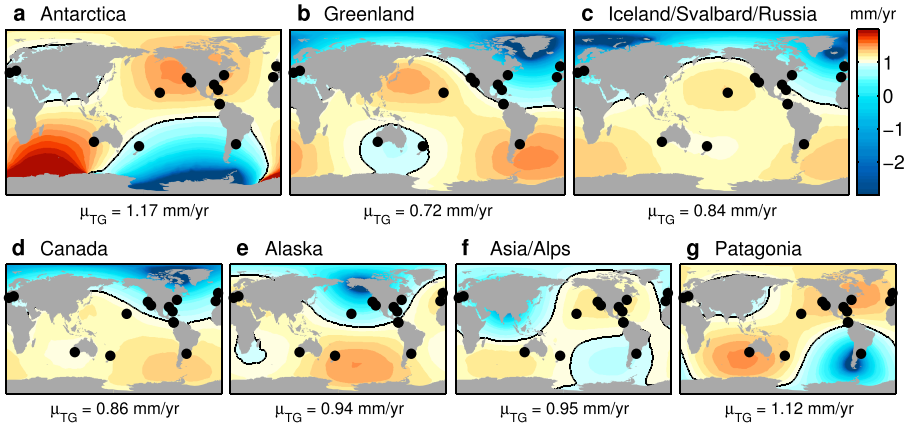

Figure 2. Gravitational melt fingerprints from GRACE on an elastic, rotating Earth. Units are sea level equivalent, and each fingerprint is normalized to have a global spatial mean of 1 mm/yr. Black contours follow the 1 mm/yr isoline, which demarcates regions with rates above and below the global mean. Calculating the mean rate at the locations of tide gauge records (μ_{TG}) represents the degree to which these locations systematically underestimate or overestimate the global mean trend associated with each melt source. (a) Antarctica, (b) Greenland, (c) Iceland/Svalbard/Russia, (d) Canada, (e) Alaska, (f) High Mountain Asia and the Alps, and (g) Patagonia.

marginal seas are not resolved in most Coupled Model Intercomparison Project Phase 5 (CMIP5) ensemble members (discussed below).

Least squares linear trends during 1901–2000 for the 15 selected records have a mean of 1.69 mm/yr and a standard deviation of 0.54 mm/yr (Figure 1a). Correcting the observed trends for GIA using the ICE-6G VM5a [*Peltier et al.*, 2015] [ICE-5G VM2 *Peltier*, 2004] model reduces the mean trend to 1.57 (1.62) mm/yr and reduces the standard deviation by more than half to 0.23 (0.24) mm/yr (Figure 1b). The consistency between the models supports the validity of the GIA corrections at these locations. The mean of the GIA-corrected twentieth century trends is consistent with mean rates from the analyses cited above, suggesting that the sampling characteristics of this core set is generally representative of the sets of long, high-quality records used in previous investigations.

3. Sources of Spatial Structure in Sea Level Change

We selected the 15 records analyzed here to minimize the effect of non-GIA vertical land motion (see Texts S1 and S2 in the supporting information). Thus, we can reasonably assume that the GIA-corrected trends from these records primarily reflect sea level rise due to a combination of global ocean volume change, ocean dynamics, and the self-attraction/loading patterns of ice melt. Depending on the spatial structure associated with the latter two contributions, the true rate of GMSL rise may be substantially greater or less than the mean trend obtained from the TG time series [*Mitrovica et al.*, 2001].

3.1. Ice Melt Fingerprints

Sea level change due to the melting of ice on land is not spatially uniform, because the Earth is a self-gravitating, viscoelastically compressible, rotating planet [*Farrell and Clark*, 1976; *Clark and Lingle*, 1977; *Lambeck*, 1980]. As a result, when an ice mass melts, sea level falls nearest the ice and rises faster than the global mean rate in the far field. The geometry of this spatial structure in sea level change is unique to each melt source and is known as a *melt fingerprint*. Here we use time-variable gravity measurements from the Gravity Recovery And Climate Experiment (GRACE) to obtain melt fingerprints on an elastic, rotating Earth during January 2003 to January 2015 [*Adhikari and Ivins*, 2016; *Adhikari et al.*, 2016]. We produce fingerprints for the Antarctic and Greenland ice sheets (Figures 2a and 2b), as well as for five geographical groupings of glaciers and ice caps thought to have contributed substantially to the twentieth century sea level rise [*Church et al.*, 2013; *Vaughan et al.*, 2013]: Iceland/Svalbard/Russia, Canada, Alaska, High Mountain Asia and the Alps, and Patagonia (Figures 2c–2g).

In general, the set of gauges used here underestimates the rate of GMSL rise due to Northern Hemisphere melt sources and overestimates the rate due to Southern Hemisphere sources. For example, 1 mm/yr of GMSL-equivalent melt from Antarctica would be recorded by this set of gauges as 1.17 mm/yr (Figure 2a), while 1 mm/yr of melt from Greenland would be recorded as just 0.72 mm/yr (Figure 2b). Based on the fingerprints of glacier and ice cap melt (Figures 2c–2g), only the Patagonia fingerprint results in a positive sampling bias, so we expect the observed TG trends to underestimate the total contribution to twentieth century global mean sea level rise from glaciers and ice caps. Thus, in order for the observed TG trends to overestimate the true rate of GMSL rise, ocean dynamics and/or ice sheet fingerprints would need to contribute a positive bias exceeding the magnitude of the negative bias from melting Northern Hemisphere glaciers and ice caps.

3.2. Ocean Dynamics

Spatial differences in long-term dynamic (i.e., related to currents and ocean density) sea level trends occur due to anthropogenic forcing and the phasing of decadal and multidecadal climate modes (e.g., the Atlantic Multidecadal Oscillation or Pacific Decadal Oscillation) [*Stammer et al.*, 2013]. Variability in winds and ocean circulation associated with these factors alters the distribution of heat and salt in the ocean, which in turn leads to spatial differences in ocean density and sea level. Unfortunately, the sparsity of hydrographic observations early in the twentieth century prevents robust estimates of spatial structure in dynamic sea level change during 1901–2000. Since we cannot know the *true* pattern of dynamic change, we use ensemble members of the Coupled Model Intercomparison Project Phase 5 (CMIP5) [*Taylor et al.*, 2012] to provide *possible* patterns of dynamic sea level change resulting from different realizations of twentieth century internal climate variability. The realism of sea level change patterns from such models is a concern, particularly at the coast due to coarse resolution, but these simulations are the best present source of information about the statistics of historical dynamic sea level change.

We calculate dynamic sea level trends (defined as the local trend minus the global mean trend) at the grid points closest to the 15 TG locations during 1901–2000 for 63 CMIP5 historical runs forced by twentieth century radiative forcing. The supporting information provides a figure summarizing the dynamic trends from the model ensemble (Figure S1). Forming ensemble averages tends to isolate the forced variability by canceling out the internal variability that is unique to each ensemble member. The absolute value of the ensemble average dynamic trends is less than 0.1 mm/yr at all but one location (Figure S1a), and the mean of the ensemble averages across the 15 locations is essentially zero (< 0.01 mm/yr). The latter quantity suggests that the forced variability does not substantially contribute to the spatial sampling bias of the 15 TG locations. In contrast, the sampling biases from each individual ensemble member are distributed in the range [−0.3, 0.3] mm/yr (Figure S1c). This demonstrates that the internal variability unique to each simulation contributes a vast majority of the potential spatial sampling bias due to twentieth century dynamic trends. It is important to note, however, that a preference for positive or negative biases does not exist in the ensemble, which is consistent with *Gregory et al.* [2001].

In order to produce a continuous distribution of spatial structure in dynamic sea level trends associated with internal variability, we first calculate empirical orthogonal functions (EOFs) of the local dynamic trends over the ensemble. The 15 resultant EOFs represent spatial structure in long-term dynamic sea level trends common to the ensemble of model runs (e.g., Figures 3a–3d). The corresponding principal components (PCs, Figure 3e) represent the amplitudes of the EOF trend patterns as a function of ensemble member rather than as a function of time as in a typical EOF decomposition. The PC amplitudes can be positive or negative depending on the phasing of the simulated internal variability in any given ensemble member. The first four EOFs account for approximately 74% of the dynamic trend variability at these locations in the 63-member ensemble. Higher-order modes have smaller amplitudes and exhibit little spatial coherence.

In general, these EOFs have nonzero means that represent the sampling bias introduced by suboptimal spatial sampling of dynamic sea level change by the 15 gauges. By generating random linear combinations of all 15 EOFs (comprising 100% of the variability), we effectively have access to an infinite number of possible dynamic patterns that might result from these models. Any single combination is unlikely to reflect the true pattern of twentieth century dynamic sea level change, but in the absence of sufficient observations, this approach allows us to use the covariance of the independent ensemble members to generate a distribution of realistic sampling biases due to ocean dynamics.

4. Estimating the Likelihood of Spatial Sampling Bias

Given the melt fingerprints from GRACE and the dynamic EOFs from CMIP5, we generate 10^6 linear combinations of these patterns with randomized amplitudes to quantify the likelihood of a systematic sampling bias in the trends from the 15 TG records. First, we determine models for the probability of possible amplitudes for each melt fingerprint and dynamic EOF (described below). Then, by drawing random values from these prescribed distributions, we search for linear combinations of the patterns that reduce scatter in the GIA-corrected TG trends. Keeping only combinations that reduce scatter reflects the reasonable assumption that at least some fraction of the variance in the GIA-corrected trends is related to ocean dynamics and melt fingerprints. We perform the search for both GIA models to assess the sensitivity of the sampling bias to the GIA correction. We perform an additional search excluding the two ice sheet fingerprints by prescribing zero melt rate to these sources. Ice sheets are the most uncertain melt contributions, and it is instructive to quantify the effect of the ice sheets on the distribution of the biases.

It is important to note that while this analysis focuses on twentieth century trends, the method does not necessarily assume that the amplitudes of the patterns are constant in time. Consider the case where instead of choosing a randomized twentieth century melt rate for each of the fingerprints, we generate a random red noise series and calculate the melt rate from the noise. Effectively, this is an identical calculation, but the red noise series will vary temporally and be uncorrelated between the different fingerprints. Thus, our method does not require melt rates from different sources to covary during the twentieth century nor does it require that the melt rates be constant. By calculating trends, we essentially filter out this independent variability between the different sources, but the method does not assume its absence.

We model the distribution of possible amplitudes for each dynamic EOF with a normal distribution defined by the standard deviation and mean of the principal component (PC) amplitudes for that EOF from the CMIP5

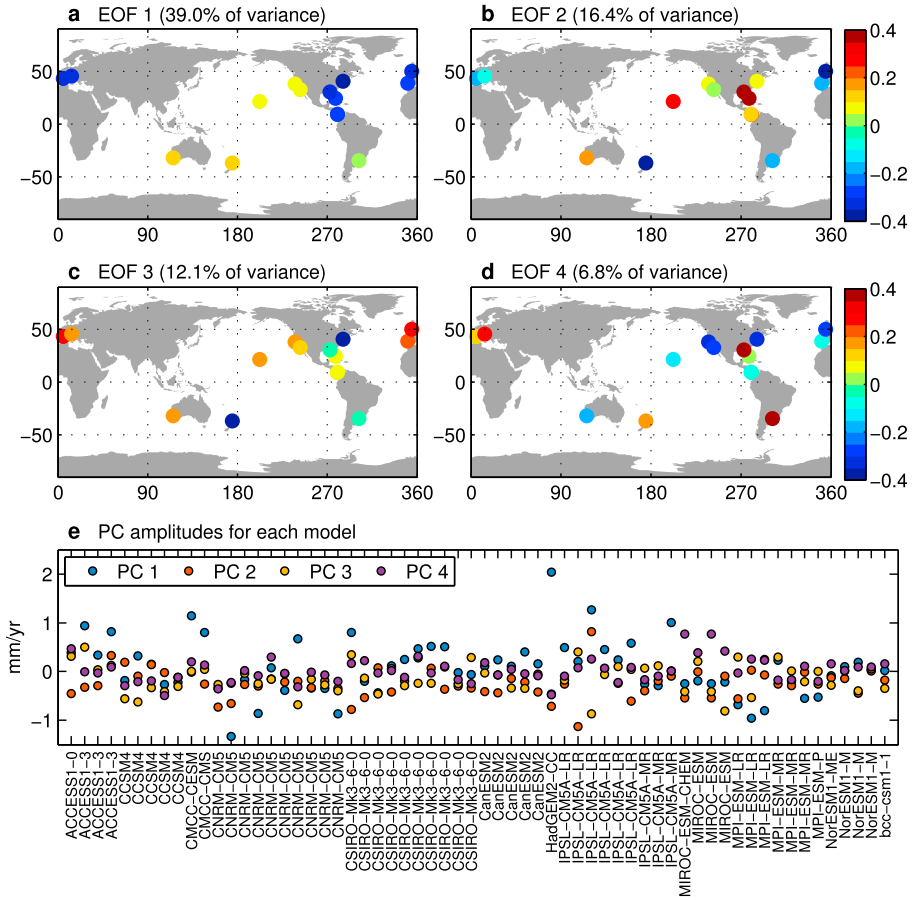

Figure 3. The first four empirical orthogonal functions (EOFs) and principal components (PCs) of CMIP5 twentieth century dynamic sea level trends at the 15 tide gauge locations. The EOFs have unit variance, while the sea level trend units are carried by the PC amplitudes. (a) EOF 1, (b) EOF 2, (c) EOF 3, (d) EOF 4, and (e) PCs 1–4 as a function of ensemble member. Repeated model names refer to different ensemble members from the same model.

ensemble members (e.g., Figure 3e). We model the distribution for possible amplitudes of the melt fingerprints based on the best available evidence from observations and models. The evidence is limited, but enough information exists to provide meaningful constraints on the fingerprint amplitudes. A synthesis of twentieth century cryospheric observations [*Vaughan et al.*, 2013; *Church et al.*, 2013] estimates that the total amount of glacier melt outside of Greenland and Antarctica has a 90% confidence range of [0.47, 0.61] mm/yr; melt from Greenland glaciers has a 90% confidence range of [0.1, 0.19] mm/yr. Observations cannot provide robust estimates of twentieth century melt from the Antarctica and Greenland ice sheets, but geodetic observations (e.g., length of day) constrain the total amount of melt from all sources to less than 1 mm/yr [*Mitrovica et al.*, 2006].

The nth randomly chosen amplitude for the kth glacial fingerprint (g_{nk}) is chosen as the sum of two normally distributed random numbers,

$$g_{nk} = \frac{t_n}{K} + x_{nk}, \tag{1}$$

where K is the number of glacier fingerprints (in this case, K=5). The random number t_n represents a possible value for the total amount of glacier melt (outside Antarctica and Greenland) during the twentieth century, which we draw from a normal distribution similar to that cited above with $\mu_t = 0.54$ mm/yr and $\sigma_t = 0.05$ mm/yr corresponding to a 90% probability range of [0.46, 0.62] mm/yr. The random number x_{nk} represents unknown scatter in the glacial melt rates, which we draw from a normal distribution centered on zero with $\sigma_x = 0.1$ mm/yr.

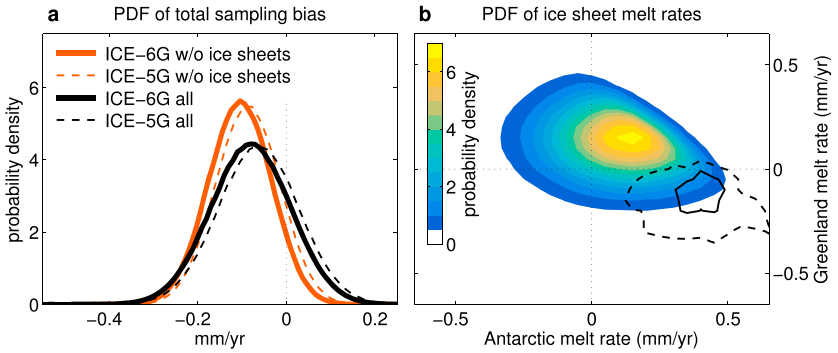

Figure 4. Tide gauge sampling bias. (a) Probability density function (PDF) of the sampling bias error for the mean of observed sea level trends (1901–2000) from 15 long tide gauge records: dynamic and all melt sources of bias (black), excluding ice sheets (orange), ICE-6G VM5a (solid), and ICE-5G VM2 (dashed). (b) PDF of ice sheet melt rates based on the observation- and model-based estimates of twentieth century melt from the Greenland and Antarctic land masses (color contours; section 4). Black contours encompass approximately 75% (dashed) and 25% (solid) of the ice sheet melt rates for sampling biases greater than 0.2 mm/yr, which tend to be related to negative Greenland melt rates (i.e., gaining mass) and/or positive Antarctic melt rates.

Upon choosing the nth set of x_{nk}, we remove the mean of the x_{nk} in order to satisfy $\sum_k g_{nk} = t_n$. This enforces the constraint that the sum of the glacial melt rates is distributed as prescribed for t_n above. Removing the mean of the x_{nk} reduces the variance of these values by a factor of $(K-1)/K$, so in practice, each x_{nk} is multiplied by $\sqrt{K/(K-1)}$ to reinflate the variance such that σ_x remains 0.1 mm/yr. This process allows for a wide range of possible amplitudes for each individual glacial fingerprint (90% probability range of [−0.03, 0.3] mm/yr) while still constraining the sum to be distributed based on observational estimates.

The melt rate of glaciers in Greenland is drawn from a distribution that mirrors the observational evidence cited above, i.e., a normal distribution centered on 0.15 mm/yr with a standard deviation of 0.03 mm/yr, which corresponds to a 90% probability range of [0.1, 0.2] mm/yr. The melt rate of the Greenland ice sheet during the twentieth century is much more uncertain, but a few model-based studies provide estimates in the range of ±0.25 mm/yr [*Gregory et al.*, 2013]. Thus, the amplitude of the Greenland fingerprint is modeled here as the sum of the randomly selected Greenland glacier melt rate plus a random number representing ice sheet melt. The latter is drawn from a normal distribution centered on zero with a standard deviation of 0.15 mm/yr corresponding to a 90% probability range of ±0.25 mm/yr.

Models of glacial-scale climate change [*Huybrechts et al.*, 2011] and an analysis of the sea level budget [*Gregory et al.*, 2013] loosely constrain the Antarctic melt rate during the twentieth century to between −0.2 and 0.5 mm/yr. Here we model the distribution of possible amplitudes for the Antarctic fingerprint as a normal distribution centered at 0.15 mm/yr with a standard deviation of 0.21 mm/yr, which corresponds to a 90% probability range of [−0.2, 0.5] mm/yr. Finally, we enforce the constraint from geodetic observations (e.g., length of day) that the total melt rate from all sources is less than 1 mm/yr [*Mitrovica et al.*, 2006]. If this final constraint is not met, we discard all the fingerprint amplitudes and draw the numbers again.

5. Results

The probability density function (PDF) for the total sampling bias in the GIA-corrected (ICE-6G VM5a) trends is centered on −0.08 mm/yr (Figure 4a), where the sign indicates that these 15 long TG records tend to underestimate the true global trend. Based on this distribution, the probability that the simple arithmetic mean of the trends from these gauges overestimates the true global rate is 19%. The probability that the observed trends overestimate the global rate by more than 0.1 mm/yr is only 2%. Using the ICE-5G GIA correction in place of the ICE-6G correction shifts the PDF toward more positive biases by almost 0.02 mm/yr. In this case, the probability that the average TG trend overestimates the true global rate is 25%, and the probability of overestimating by more than 0.1 mm/yr is 4%.

Excluding the ice sheets (by prescribing zero amplitude to the ice sheet fingerprints) while including the patterns related to ocean dynamics and glacier/ice cap melt produces comparatively narrow PDFs shifted toward more negative bias values (Figure 4a). Since the distribution of dynamic biases from the model

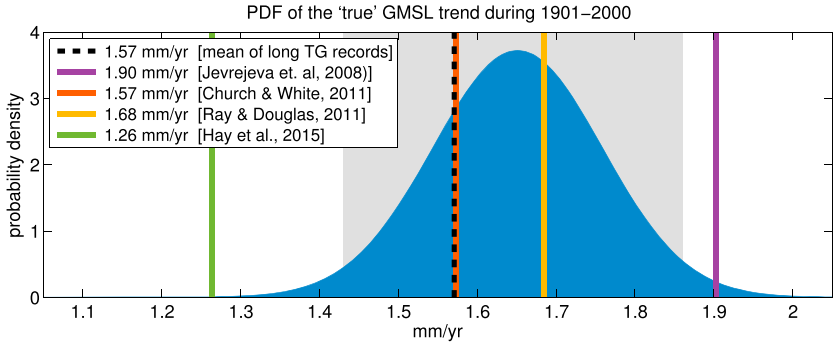

Figure 5. Probability density function (PDF) for the true rate of twentieth century GMSL rise given how the tide gauges sample spatial structure in sea level change (blue). Gray shading represents 95% confidence intervals (±0.23 mm/yr) about the central value of the distribution (1.66 mm/yr). The black dashed line shows the sample mean of the observed GIA-corrected (ICE-6G VM5a) trends from the tide gauge records; solid lines denote the linear rate of GMSL rise during 1901–2000 from four prominent twentieth century sea level reconstructions [*Jevrejeva et al.*, 2008; *Ray and Douglas*, 2011; *Church and White*, 2011; *Hay et al.*, 2015].

ensemble is centered around zero (section 3.2), the negative central value of the bias distribution is largely associated with sampling the melt fingerprints of glaciers and ice caps. This suggests that within the observation/model-based constraints, substantial contributions from the ice sheet fingerprints are by far the most likely source of large positive sampling biases. Indeed, when including the ice sheets, a vast majority (>90%) of the small number of linear combinations that produce total sampling biases greater than 0.2 mm/yr occur when both ice sheets contribute positive bias, i.e., positive Antarctic melt rate and negative Greenland melt rate (Figure 4b). Most of these combinations are unlikely, however, based on the observation- and model-based estimates of twentieth century melt from the Greenland and Antarctic land masses (section 4).

Subtracting the sampling bias from the mean of the GIA-corrected (ICE-6G VM5a) TG trends gives an estimate for the true twentieth century global mean rate of 1.66 ± 0.22 mm/yr. Using ICE-5G VM2 produces a smaller negative bias, but the mean TG rate is slightly higher, resulting in an estimate of 1.69 ± 0.22 mm/yr for the true global rate. These value represents the most likely global rate of rise when the mean TG rate is adjusted for how the gauges sample spatial structure in sea level change. The uncertainty represents a 95% confidence interval achieved by propagating the standard error of the mean and uncertainty in the sampling bias through the calculation.

Given the small number of TGs, we do not consider the global rates produced here to be a definitive estimate of twentieth century sea level rise. However, the PDF of the true global rate (blue in Figure 5) can be used to assess which reconstructions of twentieth century sea level are reasonably consistent with the longest and highest-quality TG records. Here we find that twentieth century trends from the reconstructions of *Ray and Douglas* [2011] and *Church and White* [2011] are the most consistent with trends from long, high-quality tide gauges. In contrast, the trends from *Jevrejeva et al.* [2008] and *Hay et al.* [2015] are difficult to reconcile with the tide gauge observations even after accounting for sampling bias due to spatial structure in sea level change. We note that uncertainties in reconstructed rates of twentieth century GMSL rise are large (≈0.2 mm/yr) compared to the differences between them. Nevertheless, the central estimates from these reconstructions are often used to estimate the dependence of sea level change on global temperature [*Vermeer and Rahmstorf*, 2009] (important for projections) and to provide context for the elevated rate of rise during recent decades [*Nerem et al.*, 2010].

6. Conclusions

We identify a set of the longest, highest-quality TG records and assess whether spatial structure in sea level change due to ocean dynamics or ice melt fingerprints leads to observed trends that systematically differ from the true rate of global mean sea level rise. The set of gauges utilized here tends to underestimate sea level rise due to glacier and ice cap mass loss during the twentieth century (Figure 2). Patterns of sea level change due to ocean dynamics and ice sheet melt are not likely to have amplitudes large enough to counter the effect of glacier and ice cap fingerprints and produce a positive sampling bias greater than 0.2 mm/yr (Figure 4a).

Thus, it is difficult to reconcile observed trends from the best TG records with global mean rates less than 1.4 mm/yr (Figure 5).

On their own, these results do not preclude twentieth century rates at the lower or upper end of published estimates. Without large-amplitude changes in the mass of the ice sheets, however, such rates require a physical mechanism in addition to those considered here to produce a systematic bias in relative sea level trends from long, high-quality TG records. We conclude that it is essential to reconcile statistical reconstructions of GMSL with the best available sea level observations by identifying specific physical processes that account for differences between global and local twentieth century trends.

Acknowledgments
P.R. Thompson acknowledges financial support from the NOAA Climate Program Office in support of the University of Hawaii Sea Level Center (NA11NMF4320128). B.D. Hamlington acknowledges support from the NASA New Investigator Program (NNX16AH56G). The work of F.W. Landerer and S. Adhikari was carried out at the Jet Propulsion Laboratory/California Institute of Technology, under a contract with the NASA. S. Adhikari acknowledges support from a fellowship through the NASA Postdoctoral Program. All data used in this work are freely available. Tide gauge data were obtained from the Permanent Service for Mean Sea Level (http://psmsl.org). Climate model data were obtained from the CMIP5 data portal (http://cmip-pcmdi.llnl.gov/cmip5/data_portal.html). GRACE data were obtained from the GRACE data portal (http://grace.jpl.nasa.gov/data/get-data/).

References

Adhikari, S., and E. R. Ivins (2016), Climate-driven polar motion: 2003–2015, *Sci. Adv.*, *2*(4), e1501693, doi:10.1126/sciadv.1501693.

Adhikari, S., E. R. Ivins, and E. Larour (2016), ISSM-SESAW v1.0: Mesh-based computation of gravitationally consistent sea-level and geodetic signatures caused by cryosphere and climate driven mass change, *Geosci. Model Dev.*, *9*(3), 1087–1109, doi:10.5194/gmd-9-1087-2016.

Bock, Y., S. Wdowinski, A. Ferretti, F. Novali, and A. Fumagalli (2012), Recent subsidence of the Venice Lagoon from continuous GPS and interferometric synthetic aperture radar, *Geochem. Geophys. Geosyst.*, *13*, Q03023, doi:10.1029/2011GC003976.

Brooks, B. A., M. A. Merrifield, J. Foster, C. L. Werner, F. Gomez, M. Bevis, and S. Gill (2007), Space geodetic determination of spatial variability in relative sea level change, Los Angeles basin, *Geophys. Res. Lett.*, *34*(1), L01611, doi:10.1029/2006GL028171.

Chambers, D. P. (2002), Low-frequency variations in global mean sea level: 1950–2000, *J. Geophys. Res.*, *107*(C4), 3026, doi:10.1029/2001JC001089.

Church, J. A., and N. J. White (2011), Sea-level rise from the late 19th to the early 21st century, *Surv. Geophys.*, *32*, 585–602, doi:10.1007/s10712-011-9119-1.

Church, J. A., et al. (2013), Sea level change, in *Climate Change 2013: The Physical Science Basis. Contribution of Working Group I to the Fifth Assessment Report of the Intergovernmental Panel on Climate Change*, edited by T. F. Stocker et al., pp. 1137–1216, Cambridge Univ. Press, U. K. and New York.

Clark, J. A., and C. S. Lingle (1977), Future sea-level changes due to West Antarctic ice sheet fluctuations, *Nature*, *269*(5625), 206–209, doi:10.1038/269206a0.

Douglas, B. C. (1991), Global sea level rise, *J. Geophys. Res.*, *96*(C4), 6981–6992, doi:10.1029/91JC00064.

Douglas, B. C. (1997), Global sea rise: A redetermination, *Surv. Geophys.*, *18*(2), 279–292.

Douglas, B. C. (2008), Concerning evidence for fingerprints of glacial melting, *J. Coastal Res.*, *2*, 218–227, doi:10.2112/06-0748.1.

Emery, K. O., and D. G. Aubrey (1991), *Sea Levels, Land Levels, and Tide Gauges*, 238 pp., Springer, New York.

Farrell, W. E., and J. A. Clark (1976), On postglacial sea level, *Geophys. J. R. Astron. Soc.*, *46*(3), 647–667, doi:10.1111/j.1365-246X.1976.tb01252.x.

Forbes, D. L., G. K. Manson, J. Charles, K. R. Thompson, and R. B. Taylor (2009), Halifax Harbour extreme water levels in the context of climate change: Scenarios for a 100-yr planning horizon, Open File 6346, Tech. Rep., Geol. Surv. of Canada, Ottawa.

Gregory, J. M., et al. (2001), Comparison of results from several AOGCMs for global and regional sea-level change 1900–2100, *Clim. Dyn.*, *18*(3), 225–240, doi:10.1007/s003820100180.

Gregory, J. M., et al. (2013), Twentieth-century global-mean sea level rise: Is the whole greater than the sum of the parts?, *J. Clim.*, *26*(13), 4476–4499, doi:10.1175/JCLI-D-12-00319.1.

Hamlington, B., and P. Thompson (2015), Considerations for estimating the 20th century trend in global mean sea level, *Geophys. Res. Lett.*, *42*, 4102–4109, doi:10.1002/2015GL064177.

Hay, C. C., E. Morrow, R. E. Kopp, and J. X. Mitrovica (2015), Probabilistic reanalysis of twentieth-century sea-level rise, *Nature*, *517*(7535), 481–484, doi:10.1038/nature14093.

Holgate, S. J. (2007), On the decadal rates of sea level change during the twentieth century, *Geophys. Res. Lett.*, *34*(1), L01602, doi:10.1029/2006GL028492.

Holgate, S. J., A. Matthews, P. L. Woodworth, L. J. Rickards, M. E. Tamisiea, E. Bradshaw, P. R. Foden, K. M. Gordon, S. Jevrejeva, and J. Pugh (2013), New data systems and products at the permanent service for mean sea level, *J. Coastal Res.*, *288*, 493–504, doi:10.2112/JCOASTRES-D-12-00175.1.

Huybrechts, P., H. Goelzer, I. Janssens, E. Driesschaert, T. Fichefet, H. Goosse, and M.-F. Loutre (2011), Response of the Greenland and Antarctic ice sheets to multi-millennial greenhouse warming in the Earth system model of intermediate complexity LOVECLIM, *Surv. Geophys.*, *32*(4–5), 397–416, doi:10.1007/s10712-011-9131-5.

Isla, F. I., and E. E. Toldo (2013), ENSO impacts on Atlantic watersheds of South America, *Quat. Environ. Geosci.*, *4*, 34–41, doi:10.5380/abequa.v4i1-2.33032.

Jevrejeva, S., J. C. Moore, A. Grinsted, and P. L. Woodworth (2008), Recent global sea level acceleration started over 200 years ago?, *Geophys. Res. Lett.*, *35*(8), L08715, doi:10.1029/2008GL033611.

Kirshen, P., C. Watson, E. Douglas, A. Gontz, J. Lee, and Y. Tian (2008), Coastal flooding in the Northeastern United States due to climate change, *Mitigation and Adaptation Strategies for Global Change*, *13*(5–6), 437–451, doi:10.1007/s11027-007-9130-5.

Kolker, A. S., M. A. Allison, and S. Hameed (2011), An evaluation of subsidence rates and sea-level variability in the northern Gulf of Mexico, *Geophys. Res. Lett.*, *38*, L21404, doi:10.1029/2011GL049458.

Komar, P. D., J. C. Allan, and P. Ruggiero (2011), Sea level variations along the U.S. Pacific Northwest Coast: Tectonic and climate controls, *J. Coastal Res.*, *276*, 808–823, doi:10.2112/JCOASTRES-D-10-00116.1.

Lambeck, K. (1980), *The Earth's Variable Rotation: Geophysical Causes and Consequences*, Cambridge Univ. Press, Cambridge, U. K.

Mazzotti, S., C. Jones, and R. E. Thomson (2008), Relative and absolute sea level rise in western Canada and northwestern United States from a combined tide gauge-GPS analysis, *J. Geophys. Res.*, *113*, C11019, doi:10.1029/2008JC004835.

Mitrovica, J. X., M. E. Tamisiea, J. L. Davis, and G. A. Milne (2001), Recent mass balance of polar ice sheets inferred from patterns of global sea-level change, *Nature*, *409*(6823), 1026–1029, doi:10.1038/35059054.

Mitrovica, J. X., J. Wahr, I. Matsuyama, A. Paulson, and M. E. Tamisiea (2006), Reanalysis of ancient eclipse, astronomic and geodetic data: A possible route to resolving the enigma of global sea-level rise, *Earth Planet. Sci. Lett.*, *243*(3–4), 390–399, doi:10.1016/j.epsl.2005.12.029.

Nerem, R. S., D. P. Chambers, C. Choe, and G. T. Mitchum (2010), Estimating mean sea level change from the TOPEX and Jason Altimeter Missions, *Mar. Geod.*, *33*, 435–446, doi:10.1080/01490419.2010.491031.

Peltier, W. (2004), Global glacial isostacy and the surface of the Ice-Age Earth: The ICE-5G (VM2) Model and GRACE, *Annu. Rev. Earth Planet. Sci.*, *32*(1), 111–149, doi:10.1146/annurev.earth.32.082503.144359.

Peltier, W. R., D. F. Argus, and R. Drummond (2015), Space geodesy constrains ice age terminal deglaciation: The global ICE-6G_C (VM5a) model, *J. Geophys. Res. Solid Earth*, *120*(1), 450–487, doi:10.1002/2014JB011176.

Poley, C. M., and P. Talwani (1986), Recent vertical crustal movements near Charleston, South Carolina, *J. Geophys. Res.*, *91*(B9), 9056–9066, doi:10.1029/JB091iB09p09056.

Ray, R. D., and B. C. Douglas (2011), Experiments in reconstructing twentieth-century sea levels, *Prog. Oceanogr.*, *91*(4), 496–515, doi:10.1016/j.pocean.2011.07.021.

Spada, G., and G. Galassi (2012), New estimates of secular sea level rise from tide gauge data and GIA modelling, *Geophys. J. Int.*, *191*(3), 1067–1094, doi:10.1111/j.1365-246X.2012.05663.x.

Stammer, D., A. Cazenave, R. M. Ponte, and M. E. Tamisiea (2013), Causes for contemporary regional sea level changes, *Annu. Rev. Mar. Sci.*, *5*(1), 21–46, doi:10.1146/annurev-marine-121211-172406.

Sun, H., D. Grandstaff, and R. Shagam (1999), Land subsidence due to groundwater withdrawal: Potential damage of subsidence and sea level rise in southern New Jersey, USA, *Environ. Geol.*, *37*, 290–296, doi:10.1007/s002540050386.

Taylor, K. E., R. J. Stouffer, and G. A. Meehl (2012), An overview of CMIP5 and the experiment design, *Bull. Am. Meteorol. Soc.*, *93*(4), 485–498, doi:10.1175/BAMS-D-11-00094.1.

Vaughan, D. G., et al. (2013), Observations: Cryosphere, in *Climate Change 2013: The Physical Science Basis. Contribution of Working Group I to the Fifth Assessment Report of the Intergovernmental Panel on Climate Change*, edited by T. F. Stocker et al., pp. 317–382, Cambridge Univ. Press, Cambridge, U. K. and New York.

Vermeer, M., and S. Rahmstorf (2009), Global sea level linked to global temperature, *Proc. Nat. Acad. Sci.*, *106*, 21,527–21,532, doi:10.1073/pnas.0907765106.

Wang, K. (2003), A revised dislocation model of interseismic deformation of the Cascadia subduction zone, *J. Geophys. Res.*, *108*(B1), 1–13, doi:10.1029/2001JB001227.

Wöppelmann, G., N. Pouvreau, A. Coulomb, B. Simon, and P. L. Woodworth (2008), Tide gauge datum continuity at Brest since 1711: France's longest sea-level record, *Geophys. Res. Lett.*, *35*, L22605, doi:10.1029/2008GL035783.

Wöppelmann, G., C. Letetrel, A. Santamaria, M. N. Bouin, X. Collilieux, Z. Altamimi, S. D. P. Williams, and B. M. Miguez (2009), Rates of sea-level change over the past century in a geocentric reference frame, *Geophys. Res. Lett.*, *36*, L12607, doi:10.1029/2009GL038720.

You, Z. J., D. B. Lord, and P. J. Watson (2009), Estimation of relative mean sea level rise from Fort Denison tide gauge data, in *Proceedings of the 19th Australasian Coastal and Ocean Engineering Conference*, pp. 587–592, Engineers Australia, Wellington.